The Effects of *ortho*-Phenyl Substitution on the rISC rate of D-A-Type TADF Molecules

Heather F. Higginbotham[1,‡], Chih-Lun Yi[2,‡], Andrew P. Monkman[1,*], Ken-Tsung Wong[2,3,*]

[1]Department of Physics, Durham University, South Road. DH1 3LE. [2]Department of Chemistry, National Taiwan University, Taipei 10617, Taiwan. [3]Institute of Atomic and Molecular Science, Academic Sinica, Taipei 10617, Taiwan

Two new D-A-type molecules, **PXZ-DBTO2** and **PXZ-Ph-DBTO2,** configured with phenoxazine donor and dibenzothiophene-*S*,*S*,-dioxide acceptor are reported. **PXZ-Ph-DBTO2** with a phenyl group introduced at the *ortho* position of PXZ was used to probe the effects of the congested aryl substitution on the molecular conformation and electronic coupling toward the acceptor core, as well as the thermally activated delayed fluorescence behavior. The highly twisted donor-acceptor configurations of these two molecules were confirmed by X-ray analysis. Different D-A conformations stemmed from the steric interactions between the phenyl group and acceptor core, which leads the nitrogen lone pair electrons of the **PXZ-Ph-DBTO2** donor to conjugate across the D-A bridge, whereas in **PXZ-DBTO2** the lone pairs remain localized on the donor and strongly mix with the donor π electrons. However, both **PXZ-Ph-DBTO2** and **PXZ-DBTO2** have the same energy splitting between the charge transfer states and local donor triplet states, ΔE_{ST}, close to 70 meV. **PXZ-DBTO2** exhibits far more efficient TADF due to a nearly two orders of magnitude faster reverse intersystem crossing rate as compared to that of **PXZ-Ph-DBTO2**. Detailed photophysical analysis of both molecules indicates that the presence of the phenyl group on the donor disrupts the π-π*/n-π* orbital mixing across the N-C bridge that plays a fundamental role in the excited state dynamics and vibronic coupling governing the reverse intersystem crossing rate and thus the efficiency of thermally activated delayed fluorescence. Devices employing **PXZ-DBTO2** as an emitting dopant gave an EQE of 16.7% (42 cd m^{-2}) and excellent efficiency roll-off (15.7% at 1000 cd/m^2), while the device based on **PXZ-Ph-DBTO2** produced a maxumum EQE up to 20.6% but with signifcant roll-off (8.8% at 1000 cd/m^2) ascribed to the much faster reverse intersystem crossing rate of **PXZ-DBTO2**.

‡These authors contributed to this work equally.

Introduction Organic molecules exhibiting thermally activated delayed fluorescence (TADF) are a striking class of functional materials that have been successfully utilized for high-efficiency OLEDs since the pioneering work reported by Adachi and co-workers.[1-2] It is essential, but not sufficient, for a molecule to have a small singlet (S_1)-triplet (T_1) energy splitting (ΔE_{ST}) that allows efficient reverse intersystem crossing (rISC) (T_1 state to S_1 state) to realize TADF.[3] Consequently, both singlet and triplet excitons can be efficiently harvested for light emission in TADF-based OLEDs. The critical small ΔE_{ST} generally can be achieved by subtle manipulation of the HOMO-LUMO overlap most commonly achieved in molecules with strong intramolecular charge transfer (ICT) excited states. For the last five years, a tremendous amount of new tailor-made TADF materials with sophisticated molecular structures have been studied and reported, achieving various degrees of success as they were introduced to OLED technology.[4-7] Based on the structural features of reported TADF molecules, it is generally accepted that molecules with weakly coupled donor(D)-acceptor(A) skeleton can lead to significant TADF character. In this regard, the twisted donor-acceptor configuration is one of the effective molecular design strategies for making efficient TADF molecules, as here the electron exchange energy can be minimized, yielding a small ΔE_{ST}. N-C bridged donor and acceptor moieties readily twist to impede direct electronic coupling if the significant *ortho*-*ortho* steric interactions exist between them. However, in some cases, the twisted donor-acceptor conformation can be feasibly achieved by introducing alkyl substitutions onto the donor and/or acceptor constituents as well as the π-bridge. For example, methyl group(s) was introduced onto donor moieties such as carbazoles,[8-10] phenothiazine[11] and phenylene bridges[12,13] to twist the molecular conformation and thus turn on the TADF. There are also some examples of introducing aryl group(s) that fused with the donor into a larger π-conjugated electron-donating system,[14-17] used to create a highly twisted donor-acceptor conformation. To date, there are only limited examples reported of aryl substituents introduced on the acceptor subunit based on steric repulsion considerations.[18-19] However, a second critical mechanism of TADF must also be fulfilled. To enable both reverse internal conversion (rIC) and rISC, vibronic coupling must be active to mix a local triplet excited state with the charge transfer triplet state to allow the rISC, which otherwise is formally forbidden between the singlet and triplet CT states.[20] In all CT TADF materials discovered so far, TADF is described by a second order vibronic coupled spin orbit coupling mechanism.[21] Thus, if all relative motion between D and A units is hindered by steric bulk for example, rISC is reduced by orders of magnitude and instead room temperature phosphorescence occurs.[11] Knowing this, one must be careful in the way a highly twisted D-A molecule is created so as not to impede this very important vibronic coupling mechanism.

Not only for imparting a twisted donor-acceptor conformation, we envision that an aryl substituent on the donor unit of a D-A-type ICT molecule may induce intriguing effects on the TADF behavior. Understanding the role-played by aryl substitution on the TADF behavior may also help to shed further light on the mechanism of rISC, particularly on the role of state mixing and delocalization on the donor unit. In this work, we functionalized the donor of 2-phenoxazine-dibenzothiophene-*S*,*S*,-dioxide (**PXZ-DBTO2**) with a phenyl group, attached to the *ortho*-carbon next to the nitrogen center (Scheme 1) to probe the effects of a phenyl-substituted donor on the TADF behavior. We find that the introduction of the phenyl group not only leads to a highly twisted donor-acceptor conformation, but also folds the conformation of phenoxazine (PXZ), giving a different D-A conformation compared to its parent which greatly influences the resulting electronic properties of the molecule including the dibenzothiophene-*S*,*S*,-dioxide (DBTO2) acceptor core. Detail photophysical characterizations indicate that although the ΔE_{ST} of **PXZ-Ph-DBTO2** and **PXZ-DBTO2** are both very similar at *ca.* 70 meV, the rISC rate in **PXZ-DBTO2** is nearly two orders of magnitude faster, creating far more efficient TADF and OLEDs. The mechanisms accounting for these significant differences are elucidated from our photophysical measurements.

Results and Discussion. Synthesis of target molecules **PXZ-DBTO2** and **PXZ-Ph-DBTO2**, is shown in Scheme 1. The detailed synthetic procedures and structure characterizations are reported in the Supporting Information (SI-S1). The donor (phenoxazine) 1a is commercially available. To introduce a phenyl group onto the phenoxazine, we followed a similar reported procedure[22] to prepare compound 2a, which was then subjected to a Pd-catalyzed Suzuki-Miyaura coupling reaction with phenylboronic acid, affording the intermediate 2b after the removal of the protection group with NaOMe. The target molecules, **PXZ-DBTO2** and **PXZ-Ph-DBTO2**, were then obtained in good yields by using standard Pd-catalyzed Buchwald-Hartwig amination reaction of donor 1a, 2b, and 2-bromodibenzo[*b*,*d*]thiophene 5,5-dioxide. To verify the role-played by congested phenyl substitution for governing TADF behavior, an analogue **DMAC-Ph-DBTO2**, with the same acceptor core DBTO2, but different donor (acridine), was also synthesized. All target compounds were purified by column chromatography and then vacuum sublimed before characterization and device fabrication.

Scheme 1. Synthesis of new dipolar molecules PXZ-DBTO2, PXZ-Ph-DBTO2 and the analogue DMAC-Ph-DBTO2.

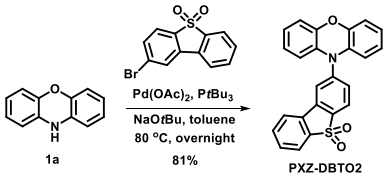

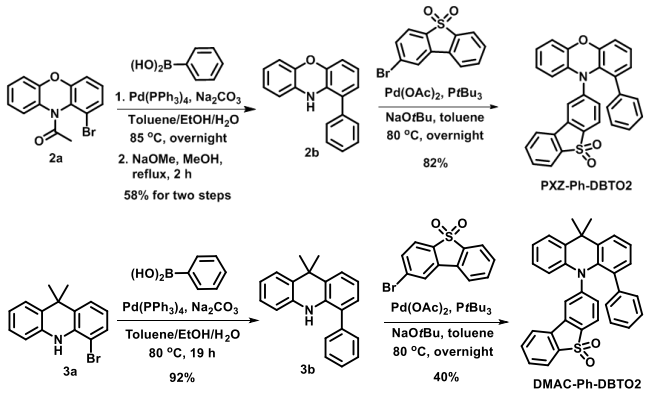

Crystal Structures. Single crystals of **PXZ-DBTO2** and **PXZ-Ph-DBTO2** suitable for X-ray diffraction analysis were obtained by a bilayer (CH_2Cl_2/hexane) diffusion method. Unfortunately, single crystals of **DMAC-Ph-DBTO2** could not be obtained. Figure 1 depicts the single crystal structures of **PXZ-DBTO2** and **PXZ-Ph-DBTO2**. The detail crystal data are summarized in Table S1 (SI). The PXZ moiety in **PXZ-DBTO2** is practically planar as expected, while the central ring of PXZ in **PXZ-Ph-DBTO2** exhibits a distorted boat conformation. **PXZ-DBTO2** exhibits a highly twisted D-A conformation with a dihedral angle of 66.5° between the PXZ and DBTO2 core, presumably due to the typical *ortho-ortho* hydrogen-to-hydrogen steric interactions. The PXZ in **PXZ-Ph-DBTO2** is folded along the N···S axis, creating a dihedral angle of ~130.8°. The folded conformation can be mainly attributed to the large steric interaction between the phenyl group and DBTO2 core but also through an electronic effect in the donor unit. The distorted boat-shape of PXZ and resulting D-A structure, closely resembles observed conformations in phenothiazine[20] and *ortho*-methyl-substituted phenothiazine TADF molecules.[11] In addition, the dihedral angle between the phenyl group and PXZ of **PXZ-Ph-DBTO2** is calculated to be 48.4°. As observed in the **PXZ-Ph-DBTO2** crystal, the boat configuration leads to a highly twisted D-A configuration where the nitrogen lone-pair electrons of the PXZ unit to align favorably for better π-conjugation with the DBTO2 rather than with the phenylene rings of PXZ. Thus, the N-C (DBTO2) bond, 0.027 Å, is shorter than the N-C (PXZ) bonds, 0.028 Å, while the N-C (DBTO2) bond, 0.022 Å, in **PXZ-DBTO2** is longer than N-C (PXZ) bond, 0.019 Å. The configuration of the parent **PXZ-DBTO2** molecule can be described as quasi-equatorial, while the **PXZ-Ph-DBTO2** it is quasi-axial configuration. Such configurational forms are discussed in detail in reference.[20] Whilst in both conformers the D and A are near orthogonal, the nitrogen lone pairs are oriented in different directions with respect to the acceptor unit in the two cases, with the axial conformer giving greater conjugation between donor and acceptor unit, whereas the equatorial conformer prevents such delocalization of the nitrogen lone pair with the acceptor giving instead strong nπ mixing within the donor unit. The result implies that these two molecules have a different degree of electronic coupling between the donor and acceptor units.

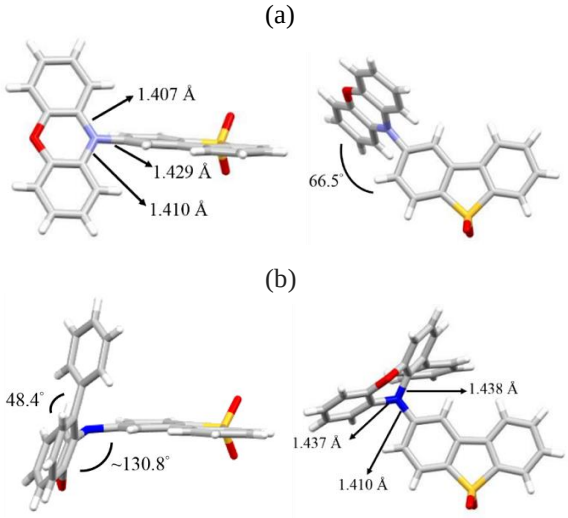

Figure 1. X-ray structures of (a) PXZ-DBTO2 and (b) PXZ-Ph-DBTO2.

Thermal and Electrochemical Properties. Thermal stability of these compounds were analyzed by thermogravimetric analysis (TGA). The decomposition temperature (T_d, corresponding to 5% weight loss) for **PXZ-DBTO2**, **PXZ-Ph-DBTO2** and **DMAC-Ph-DBTO2**, was determined to be 319, 300 and 311 °C, respectively (Figure S3 in SI). All these compounds exhibit sufficient thermal stability for the thin films preparation by thermal evaporation. In addition, the analysis by differential scanning calorimetry (DSC) indicated that **PXZ-Ph-DBTO2** and **DMAC-Ph-DBTO2** exhibit a glass transition temperature (T_g) of 106 and 137 °C (Figure S4 in SI), respectively. Cyclic voltammetry (CV) of **PXZ-DBTO2**, **PXZ-Ph-DBTO2**, **DMAC-Ph-DBTO2**, all display quasi-reversible oxidation with potentials of 0.92, 1.04, and 1.23 V and reduction potentials at -1.52, -1.63, and -1.79 V, respectively, indicating their bipolar electrochemical characteristics (Figure S5 in SI). Referenced to the redox potential of ferrocene, the HOMO/LUMO levels of **PXZ-DBTO2**, **PXZ-Ph-DBTO2** and **DMAC-Ph-DBTO2** were calculated from their respective oxidation/reduction potentials to be -5.20/-2.73 eV, -5.36/-2.56 eV and -5.55/-2.53 eV, respectively. Compared to **PXZ-DBTO2**, it is obvious that the introduction of phenyl substitution at the *ortho* position of the donor PXZ leads to a lower HOMO level and higher LUMO level as observed in **PXZ-Ph-DBTO2**. This result clearly indicates the weaker electron-donating character of the phenyl-substituted phenoxazine as compared to that of phenoxazine, which is consistent with the observation from the **PXZ-Ph-DBTO2** crystal structure where the axial conformation causes the electron-donating N-center in the phenyl-substituted phenoxazine to have increased conjugation with the DBTO2 acceptor core. The effect of *ortho*-phenyl substitution on the electronic character of DBTO2 was also observed in **DMAC-Ph-DBTO2**, giving a similar LUMO level as compared to that of **PXZ-Ph-DBTO2**.

Steady State Spectroscopy. The UV-visible spectra of **PXZ-Ph-DBTO2** and **PXZ-DBTO2** display some similari-

ties, with high energy transitions at ~318 nm and 275 nm, seen in all solvents (Figure 2). The molar absorptivity coefficients of the 318 nm transition in dichloromethane (DCM) is markedly different however, being 6,450 (L mol^{-1} cm^{-1}) for **PXZ-Ph-DBTO2** and 11,260 (L mol^{-1} cm^{-1}) for **PXZ-DBTO2** (Figures S6 and S7 in SI). Such a strong molar absorptivity and the observed positive solvatochromism attests to the strong π-π* character of this transition. **PXZ-Ph-DBTO2** also displays an additional high energy transition at ~280 nm, mixed into the strongly vibronic 275 nm absorption. This is most likely an absorbance from the phenyl moiety, substituted at the *ortho*-position of the donor PXZ. All high energy bands (> 280 nm) in both materials absorb strongly (> 10,000 L mol^{-1} cm^{-1}) and can therefore also be assigned to transitions with π-π* character.

Interestingly, in **PXZ-DBTO2**, a strong low energy band is observed between ~350-480 nm that is not visible in **PXZ-Ph-DBTO2** (Figure 2). This broad absorption has a molar absorptivity coefficient of 1,240 L mol^{-1} cm^{-1} (Figure S7) and can, therefore, be ascribed to a direct CT transition with mixed π-π/n-π* character.[23] While this band is not observed in **PXZ-Ph-DBTO2** a low energy knee between ~350-385 nm with a similar molar absorptivity coefficient (1,140 L mol^{-1} cm^{-1} at 370 nm in DCM of Figure S6) is present. This blue spectral shift of the CT transition and large redistribution of oscillator strength caused by the addition of the phenyl group clearly shows a marked redistribution of the nitrogen lone pairs across the D-A bridge and concomitant change in the degree of π-π/n-π* orbital mixing, dramatically effecting the direct CT transition. These marked structural and electronic changes are induced by the substituent phenyl ring, whereas previously we have observed two different conformer structures only in regio-isomers of a phenothiazine-DBTO2 TADF molecule, where delocalization of the nitrogen lone pairs is controlled by the *ortho* or *para* coupling of the D-A units.[20] In the case of **PXZ-DBTO2/ PXZ-Ph-DBTO2** pair, the different conformers are caused by donor substitution.

In order to prove that these effects are caused by the phenyl moiety on the donor unit, the analogue **DMAC-Ph-DBTO2** was also investigated. Here we find that the same low energy band (molar absorptivity coefficient = 1,100 L mol^{-1} cm^{-1} at 380 nm in DCM (inset of Figure S8 in SI) with low absorptivity is present while the main donor transition at 330 nm (9,550 L mol^{-1} cm^{-1} in DCM (Figure S8 in SI) with π-π* character is also observed (Figure S9 in SI). **DMAC-Ph-DBTO2**, therefore, shows very similar low energy characteristics to that of **PXZ-Ph-DBTO2**.

The emission spectra of each material in non-polar methylcyclohexane (MCH) (ε = 2.05) reveals a slightly structured band with onset energies of 428 nm (2.89 eV) and 439 nm (2.82 eV) in **PXZ-Ph-DBTO2** and **PXZ-DBTO2** respectively; energies that suggest a mixture of ^{1}LE (donor) and ^{1}CT character.[24] These spectra show that the phenyl group on **PXZ-Ph-DBTO2** does not add additional conjugation to the donor rings and subsequently the expected bathochromic shift in **PXZ-Ph-DBTO2** is not observed. Additionally, **PXZ-Ph-DBTO2** and **PXZ-DBTO2** show strong positive solvatochromism and Gaussian emission profiles indicative of charge transfer character.[4-5,25] The energy onset shift between each material in different solvents is larger in **PXZ-DBTO2**, 0.22 eV, compared to **PXZ-Ph-DBTO2**, 0.18 eV (between the emission onset in toluene and chloroform) implying a larger dipole moment (degree of charge transfer) in the former. This shows that conjugation between D and A diminishes the change in dipole moment on excitation and hence the degree of charge transfer character of the excited state. Furthermore, contrary to normal CT behavior the emission intensity does not simply decrease with increasing solvent polarity. This is especially prominent in **PXZ-DBTO2** where the emission in toluene is greatly enhanced compared to all other solvents (Figure 2). The maxima in emission intensity is found to coincide with the smallest ΔE_{ST} and hence strongest triplet harvesting *via* TADF, *i.e.* when the onset of emission coincides with the onset of the phosphorescence of **PXZ-DBTO2** as given in fig. 4., where ΔE_{ST} is a minimum. We therefore deduce that the prominent deactivation pathway as the CT shifts to lower energy (in higher polarity) in these materials is through (unharvested) ^{3}CT triplet state production.

Degassing these materials in toluene shows an increase in intensity that indicates a population of the triplet states which contribute to the overall luminescence. From these degassed (prompt + delayed emission) and aerated (prompt emission only) spectra we find that delayed emission contributes strongly to the overall intensity of the spectrum (DF/PF=5.4) in **PXZ-DBTO2**, while this contribution is greatly diminished in **PXZ-Ph-DBTO2** (DF/PF=1.0) (Figure S10 in SI). This provides evidence that rISC in **PXZ-DBTO2** is more efficient than in **PXZ-Ph-DBTO2**.

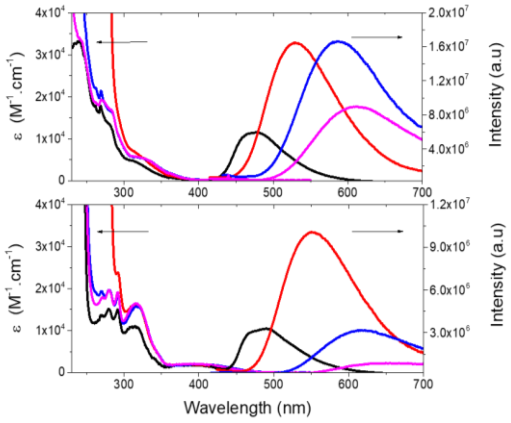

Figure 2. Top: Absorbance and emission (λ_{ex}=320 nm) spectra of 20 μM **PXZ-Ph-DBTO2**. Bottom: Absorbance and emission (λ_{ex}=360 nm) spectra of 20 μM **PXZ-DBTO2**. Solvents methylcyclohexane (black), toluene (red), chloroform (blue) and dichloromethane (pink).

In solid state (1% w/w ratio in inert zeonex matrix) the same general absorption spectra are observed (Figure S11), however the steady state emission is rather different. In both phenyl substitutes **PXZ-Ph-DBTO2** and **DMAC-Ph-DBTO2** materials ^{1}LE emission (3.1 eV) is observed along

with the strong CT band (as seen in solution Figure 2). However, in the **PXZ-DBTO2** only the CT emission band is seen. This clearly indicates that in the restricted environment of the zeonex matrix D rotation to the stabilized CT geometry (potentially an axial to equatorial isomerization) is hindered giving rise to the dual emission.

Time Resolved/Temperature Dependent Spectroscopy. Both **PXZ-Ph-DBTO2** and **PXZ-DBTO2** films cast in zeonex were analyzed using time-resolved/temperature dependent photoluminescence spectroscopy (Figure 3). Both solid-state samples were analyzed between 1 ns and 79 ms at temperatures between 80 K and 300-320 K in order to understand the excited states involved in photoluminescence decay process. Firstly, both materials decay in two distinct time regions; one between 1-100 ns (prompt CT emission)[26] and one found at later delay times (>100 ns). In the prompt region of **PXZ-Ph-DBTO2**, the decay fits to two exponentials, 1.3±0.2 ns, and 8.5±0.4 ns. These two lifetimes can be attributed to emission from the ^{1}LE and ^{1}CT state, confirmed upon inspection of the spectra in this time region (Figure S12 in SI). Furthermore, throughout the whole prompt region, the spectra bathochromically shift showing extremely slow excited state relaxation (Figure S12a)[23] The prompt decay of **PXZ-DBTO2** can also be fitted to two exponentials of 8.8±0.4 ns and 27±2 ns. However, the spectra of **PXZ-DBTO2** show no evidence of ^{1}LE and little spectral relaxation displaying an almost identical spectral shape and onset energy from TD=1 ns through to the delayed emission region. (Figure S12b in SI).

From the temperature dependence of the time-resolved spectra of these two materials, both materials show delayed emission (shown to be TADF by the linear dependence of the delay emission with laser excitation intensity (Figure S13 in SI)). However, the delayed fluorescence observed from **PXZ-DBTO2** is much stronger and the lifetime of this delayed component is much shorter than **PXZ-PH-DBTO2**. The lifetime of the delayed emission (emission of > 100 ns and therefore assume to be the photons emitting after at least one excursion to the triplet state) at 300 K was found to be 6.5 ± 0.4 µs for **PXZ-DBTO2**, and 76 ± 4 µs for **PXZ-Ph-DBTO2**; an order of magnitude slower than **PXZ-DBTO2**. This is further reflected in the calculated rISC rates ($k_{rISC} = \frac{I_{DF}}{I_{PF}}\frac{1}{\tau_{TADF}}$) for the two materials, 1.3×10^4 s^{-1} for **PXZ-Ph-DBTO2** and 7.7×10^5 s^{-1} for **PXZ-DBTO2**; the latter rate implying close to resonant behavior between the ^{1}CT-^{3}LE excited states.[6,20] The contrast in TADF output between the two materials is at first difficult to explain from initial inspection of the associated spectra at each delay time. Here we find that both materials contain ^{1}CT excited states in close proximity to a local triplet state (obtained from phosphorescence recorded at low temperatures and long delay times > 40 ms, Figure 3-pink spectra), with the ΔE_{ST} of **PXZ-Ph-DBTO2** and **PXZ-DBTO2** found to be 70 and 68 meV respectively (Figure 3). This should therefore imply that both emitters are equally strong TADF materials with comparable rISC rates.

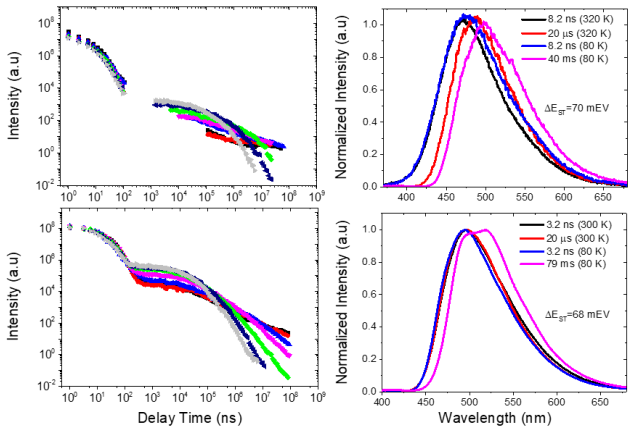

Figure 3. Top left: Emission intensity against delay time measured at 80 K (black), 120 K (red), 160 K (blue), 200 K (pink), 240 K (green), 280 K (navy), 320 K (grey) of 1% w/w **PXZ-Ph-DBTO2** in zeonex. Top right: Normalized intensity spectra at both 320 K and 80 K of 1% w/w **PXZ-Ph-DBTO2** in zeonex. Bottom left: Emission intensity against delay time measured at 80 K (black), 120 K (red), 160 K (blue), 200 K (pink), 240 K (green), 280 K (navy), 300 K (grey) of 1% w/w **PXZ-DBTO2** in zeonex. Bottom right: Normalized intensity spectra at both 300 K and 80 K of 1% w/w **PXZ-DBTO2** in zeonex.

Triplet State Analysis. Although the ΔE_{ST} of both **PXZ-Ph-DBTO2** and **PXZ-DBTO2** are both close to 70 meV, we find that the rISC rate in **PXZ-DBTO2** is nearly two orders of magnitude faster, creating far more efficient TADF. This phenomenon cannot be explained without a detailed exploration of the triplet states that contribute to the dynamics of the rISC process, Figure 3. While the triplet state of **PXZ-DBTO2** (onset energy = 2.70 eV, Figure 3 bottom/right spectra) is very similar to that of the PXZ donor itself (^{3}LE$_D$)[24], the **PXZ-Ph-DBTO2** triplet emission (onset energy = 2.82 eV, Figure 3 top/right spectra) has characteristics of both the PXZ donor *and* the DBTO2 acceptor (^{3}LE$_A$).[27] Taking the difference between the **PXZ-Ph-DBTO2** (Figure 4-black spectrum) and the **PXZ-DBTO2** phosphorescence spectra (Figure 4-red spectrum) yields an emission component (Figure 4-blue spectrum) which has the same energy peak maximum (2.66 eV) and vibrational shape as the DBTO2 acceptor shown by Nobuyasu et. al.[27] in the identical host matrix. The lifetime of **PXZ-Ph-DBTO2**'s two emissive triplet states cannot be deconvolved from one another, e.g. at no point in the emission decay can a single phosphorescence spectrum be seen, Figure S14, and the overall spectral shape of the triplet emission does not change, as was also found by Nobuyasu et. al.[27] implying that both the donor and the acceptor triplet states are vibrationally coupled.[21,26]

To further corroborate this observation, an identical time-resolved/temperature dependent analysis was performed on the analogue **DMAC-Ph-DBTO2** (Figure S15 in SI). Here we find that the phosphorescence of **DMAC-Ph-DBTO2** is spectrally almost identical to **PXZ-Ph-DBTO2**, indicating that the difference in triplet state behavior between **PXZ-Ph-DBTO2** and **PXZ-DBTO2** is due to the phenyl ring on the donor unit, not the magnitude of ΔE_{ST},

which in **DMAC-Ph-DBTO2** is very much larger, *ca.* 0.37 eV. In these two cases the conjugation of the nitrogen lone pair across the D-A bridge is the common factor giving rise to this coupled triplet state behavior, as it is not seen in **PXZ-DBTO2**.

This ^3LE_A state is naturally still present in **PXZ-DBTO2**, however, its absence in the phosphorescence spectra implies it is not coupled to the ^3LE_D and is simply quenched by this lower energy triplet state.[21] This implies that regardless of the energy splitting between the singlet and triplet states, ΔE_{ST} which is the same in these two materials, the second-order vibronically coupled spin orbit coupling between the ^{1}CT state and the ^3LE_D in **PXZ-DBTO2** is far more efficient than within **PXZ-Ph-DBTO2**, accounting for the two orders of magnitude difference in the rISC rates. We therefore propose that the coupling between the ^3LE_D and ^3LE_A local triplets competes with the ^{3}CT-^3LE_D coupling. This competition between state couplings affects the mediating role of the ^3LE_D in the overall rISC mechanism[21] and slows down the rISC rate by nearly two orders of magnitude.

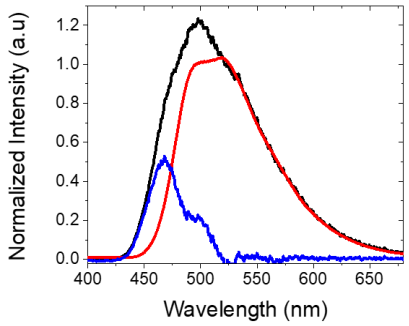

Figure 4. Normalized phosphorescence spectrum of **PXZ-Ph-DBTO2** (black), and **PXZ-DBTO2** (red) and the energy difference between them (blue)

This fundamental difference in decay pathway between **PXZ-Ph-DBTO2** and **PXZ-DBTO2** is further reflected on inspection of OLED devices performance. OLEDs were prepared using vacuum deposition using the following optimized device architecture: ITO/NPB (40 nm)/ 15% emitter:mCP (30 nm)/ TPBi (40 nm)/ BCP (10 nm)/ LiF (1 nm)/ Al (100 nm). mCP was used as a host due to its high energy triplet (2.9 eV) in order to facilitate triplet exciton localization upon the emitter molecule. Both emitters in mCP host have green electroluminescence with **PXZ-DBTO2** shifted slightly more to the red, directly in line, with similar energies to that of the materials in toluene solvent. As seen in the solvent series displayed in Figure 2 **PXZ-DBTO2** is the more bathochromically shifted of the two materials, further displaying its stronger CT characteristics even within thin film host. Figure 5 shows stark differences between the two emitters used. Both devices show low turn-on voltages (Figure S16 in SI) showing good charge balance and localization of hole and electrons into the emitter layer.

Although **PXZ-Ph-DBTO2** has an EQE maximum of 20.6% at a luminance of 43 cd m^{-2} (10 cd m^{-2}), a step roll-off in luminance and current efficiency is observed. On the other hand, the device of **PXZ-DBTO2** produced an EQE of 16.7% at a luminance of 42 cd m^{-2} (10 cd m^{-2}), however, minimal roll-off (showing almost identical EQE at both 100 and 1000 cd m^{-2}) and device stability is observed (Table 1). From the cyclic voltammetry measurements, we find that the LUMO level of **PXZ-DBTO2** (-2.73 eV) is well placed for direct injection of electrons from the electron transporting material (TPBi) (LUMO = -2.7 eV). This may, in turn, compensate for the superior hole injection properties of the mCP host, and therefore may account for the enhanced OLED characteristics seen in **PXZ-DBTO2**. However, the excellent roll-off characteristics of the **PXZ-DBTO2** devices can be attributed to the two orders of magnitude faster rISC rate and more efficient TADF.

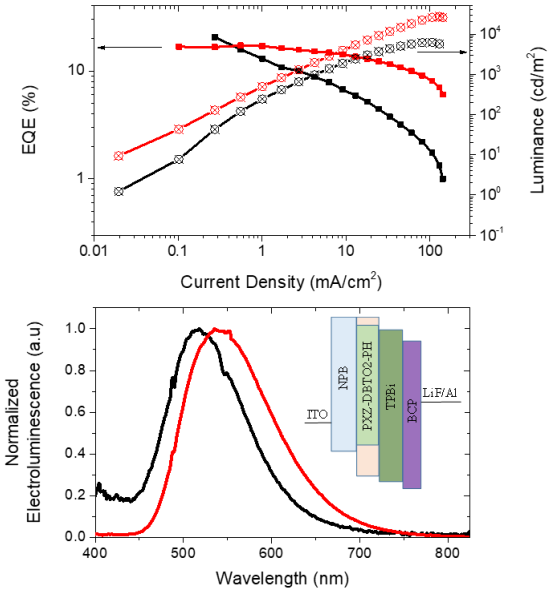

Figure 5. **PXZ-Ph-DBTO2**/PXZ-DBTO2:mCP OLED characteristics. Top: EQE versus current density (left axis) and luminance versus current density (right axis) of **PXZ-Ph-DBTO2** (black) and **PXZ-DBTO2** (red) Bottom: Normalized electroluminescence of **PXZ-Ph-DBTO2** (black) and **PXZ-DBTO2** (red), inset: device structure of **PXZ-Ph-DBTO2** device as a representation of HOMO–LUMO energy levels of each layer.

Table 1. OLED characteristics of PXZ-Ph-DBTO2 and PXZ-DBTO2 devices at a luminance of 100, 1000 and 10,000 cd.m^{-2}

	Luminance (cd/m^2)	Voltage (V)	EQE (%)	Current Efficiency (cd/A)
PXZ-Ph-DBTO2	100	5.4	15.8	34.5
	1000	7.5	8.8	25.1
	10000	-	-	-
PXZ-DBTO2	100	4.8	16.6	46.3
	1000	6.7	15.7	46.0
	10000	10.2	11.5	34.9

Conclusion A simple phenyl substituent on the phenoxazine donor unit of **PXZ-DBTO2**, leads to major changes in both the conformer structure of the resultant molecule, **PXZ-Ph-DBTO2**, and TADF parameters. The quasi-axial conformation of **PXZ-Ph-DBTO2** redistributes the donor nitrogen lone pair across the D-A bridge

whereas in **PXZ-DBTO2** the lone pair is strongly mixed with the donor π orbitals and remains decoupled from the acceptor unit. We find that this gives rise to a near two orders of magnitude increase in the rISC rate of **PXZ-DBTO2** whilst the singlet triplet splitting, ΔE_{ST}, remains unaffected. Moreover, the conjugation of the lone pair across the D-A bridge acts to enhance the vibrational coupling between donor and acceptor local triplet states leading to clear dual phosphorescence with both triplet states emitting at the same decay rate. We believe that this triplet state coupling competes with the vibronic coupling between the donor local triplet and the CT states reducing the rISC rate. Hence, again we show that the ΔE_{ST} does not simply control rISC; vibronic coupling between local triplet and CT states is just as important. This behavior then manifests itself in OLED devices where the faster rISC rate leads to far superior roll-off characteristics and device efficiency. Thus, a simple substitution on a donor to control steric properties or triplet energy etc. clearly can have far more important ramifications in the complex second order vibronically coupled spin orbit coupling mechanism underlying rISC in the TADF process.

ASSOCIATED CONTENT

Supporting information. This material is available free of charge via the Internet at http://pubs.acs.org.
Experimental methods, X-ray crystallography, characterization data, cyclic voltammetry, additional steady state and time resolved spectroscopic data, additional OLED characterization data.

AUTHOR INFORMATION

Corresponding Author

* a.p.monkman@durham.ac.uk; kenwong@ntu.edu.tw

Author Contributions

The manuscript was written through contributions of all authors. All authors have given approval to the final version of the manuscript. ‡H.F.H and C.Y contributed equally to this work.

Funding Sources

The authors acknowledge financial support from the Ministry of Science and Technology (Grant Nos. MOST 104-2113-M-002-006-MY3) and A.P.M and H.F.H. acknowledge the EU's Horizon 2020 for funding the PHEBE project under grant no. 641725. A.P.M. acknowledges the EPSRC for funding under grant number EP/L02621X/1. Part of the work was supported by the EU's Horizon 2020 funding the OCTA project under grant agreement No 778158

Notes

The authors declare no competing financial interests.

ACKNOWLEDGMENT

REFERENCES

(1) Endo, A.; Ogasawara, M.; Takahashi, A.; Yokoyama, D.; Kato, Y. Thermally Activated Delayed Fluorescence from Sn^{4+}–Porphyrin Complexes and Their Application to Organic Light Emitting Diodes — A Novel Mechanism for Electroluminescence. *Adv. Mater.* **2009**, *21*, 4802.
(2) Uoyama, H.; Goushi, K.; Shizu, K.; Nomura, H.; Adachi, C. Highly Efficient Organic Light-Emitting Diodes from Delayed Fluorescence. *Nature* **2012**, *492*, 234.
(3) Dias, F. B.; Bourdakos, K. N.; Jankus, V.; Moss, K. C.; Kamtekar, K. T.; Bhalla, V.; Santos, J.; Bryce, M. R.; Monkman, A. P. Triplet Harvesting with 100% Efficiency by Way of Thermally Activated Delayed Fluorescence in Charge Transfer OLED Emitters. *Adv. Mater.* **2013**, *25*, 3707.
(4) Tao, Y.; Yuan, K.; Chen, T.; Xu, P.; Li, H.; Chen, R.; Zheng, C.; Zhang, L.; Huang, W. Thermally Activated Delayed Fluorescence Materials Towards the Breakthrough of Organoelectronics. *Adv. Mater.* **2014**, *26*, 7931.
(5) Yang, Z.; Mao, Z.; Xie, Z.; Zhang, Y.; Liu, S.; Zhao, J.; Xu, J.; Chi, Z.; Aldred, M. P. Recent Advances in Organic Thermally Activated Delayed Fluorescence Materials. *Chem. Soc. Rev.* **2017**, *46*, 915.
(6) Dias, F. B.; Penfold, T. J.; Monkman, A. P. Photophysics of Thermally Activated Delayed Fluorescence Molecules. *Methods Appl. Fluoresc.* **2017**, *5*, 012001.
(7) Wong, M. Y.; Zysman-Colman, E. Purely Organic Thermally Activated Delayed Fluorescence Materials for Organic Light-Emitting Diodes. *Adv. Mater.* **2017**, *29*, 1605444.
(8) Park, I. S.; Lee, S. Y.; Adachi, C.; Yasuda, T. Full-Color Delayed Fluorescence Materials Based on Wedge-Shaped Phthalonitriles and Dicyanopyrazines: Systematic Design, Tunable Photophysical Properties, and OLED Performance. *Adv. Funct. Mater.* **2016**, *26*, 1813.
(9) Lee, J.; Aizawa, N.; Numata, M.; Adachi, C.; Yasuda, T. Versatile Molecular Functionalization for Inhibiting Concentration Quenching of Thermally Activated Delayed Fluorescence. *Adv. Mater.* **2017**, *29*, 1604856..
(10) Numata, M.; Yasuda, T.; Adachi, C. High Efficiency Pure Blue Thermally Activated Delayed Fluorescence Molecules Having 10*H*-Phenoxaborin and Acridan Units. *Chem. Commun.* **2015**, *51*, 9443.
(11) Ward, J. S.; Nobuyasu, R. S.; Batsanov, A. S.; Data, P.; Monkman, A. P.; Dias, F. B.; Bryce, M. R. The Interplay of Thermally Activated Delayed Fluorescence (TADF) and Room Temperature Organic Phosphorescence in Sterically-Constrained Donor–Acceptor Charge-Transfer Molecules. *Chem. Commun.* **2016**, *52*, 2612.
(12) Liu, Y.; Xie, G.; Wu, K.; Luo, Z.; Zhou, T.; Zeng, X.; Yu, J.; Gong, S.; Yang, C. Boosting Reverse Intersystem Crossing by Increasing Donors in Triarylboron/Phenoxazine Hybrids: TADF Emitters for High-Performance Solution-ProcesseOLEDs. *J. Mater. Chem. C* **2016**, *4*, 4402.
(13) Cui, L.S.; Nomura, H.; Geng, Y.; Kim, J. U.; Nakanotani, H.; Adachi, C. Controlling Singlet–Triplet Energy Splitting for Deep-Blue Thermally Activated Delayed Fluorescence Emitters. *Angew. Chem. Int. Ed.* **2017**, *56*, 1571.
(14) Endo, A.; Sato, K.; Yoshimura, K.; Kai, T.; Kawada, A.; Miyazaki, H.; Adachi, C. Efficient Up-Conversion of Triplet Excitons into a Singlet State and Its Application for Organic Light Emitting Diodes. *Appl. Phys. Lett.* **2011**, *98*, 083302.
(15) Yoo, S. G.; Song, W.; Lee, J. Y. Molecular Engineering of Donor Moiety of Donor–Acceptor Structure for Management of Photophysical Properties and Device Performances. *Dyes Pigm.* **2016**, *128*, 201.
(16) Sato, K.; Shizu, K.; Yoshimura, K.; Kawada, A.; Miyazaki, H.; Adachi, C. Organic Luminescent Molecule with Energetically Equivalent Singlet and Triplet Excited States for Organic Light-Emitting Diodes. *Phys. Rev. Lett.* **2013**, *110*, 247401.
(17) Zhang, D. Song, X.; Cai, M.; Kaji, H.; Duan, L. Versatile Indolocarbazole-Isomer Derivatives as Highly Emissive Emitters and Ideal Hosts for Thermally Activated Delayed Fluorescent

OLEDs with Alleviated Efficiency Roll-Off. *Adv. Mater.* **2018**, DOI:10.1002/adma.201705406.
(18) Chen, D.Y.; Liu, W.; Zheng, C.J.; Wang, K.; Li, F.; Tao, S. L.; Ou, X.-M.; Zhang, X.H. Isomeric Thermally Activated Delayed Fluorescence Emitters for Color Purity-Improved Emission in Organic Light-Emitting Devices. *ACS Appl. Mater. Interf.* **2016**, *8*, 16791.
(19) Wang, K.; Zheng, C.-J.; Liu, W.; Liang, K.; Shi, Y.-Z.; Tao, S. L.; Lee, C. S.; Ou, X.-M.; Zhang, X.H. Avoiding Energy Loss on TADF Emitters: Controlling the Dual Conformations of D–A Structure Molecules Based on the Pseudoplanar Segments. *Adv. Mater.* **2017**, *29*, 1701476.
(20) Etherington, M. K.; Gibson, J.; Higginbotham, H. F.; Penfold, T. J.; Monkman, A. P. Revealing the Spin–Vibronic Coupling Mechanism of Thermally Activated Delayed Fluorescence. *Nat. Commun.* **2017**, 13680.
(21) Gibson, J.; Monkman, A. P.; Penfold, T. J. The Importance of Vibronic Coupling for Efficient Reverse Intersystem Crossing in Thermally Activated Delayed Fluorescence Molecules. *ChemPhysChem* **2016**, *17*, 2956.
(22) Thomé, I.; Bolm, C. Transition-Metal-Free Intramolecular *N*-Arylations. *Org. Lett.* **2012**, *14*, 1892-1895.
(23) dos Santos, P. L.; Ward, J. S.; Bryce, M. R.; Monkman, A. P. Using Guest–Host Interactions To Optimize the Efficiency of TADF OLEDs. *J. Phys. Chem. Lett.* **2016**, *7*, 3341.
(24) dos Santos, P. L.; Ward, J. S.; Data, P.; Batsanov, A. S.; Bryce, M. R.; Dias, F. B.; Monkman, A. P. Engineering the Singlet–Triplet Energy Splitting in a TADF Molecule. *J. Mater. Chem. C* **2016**, *4*, 3815.
(25) Volz, D.; Wallesch, M.; Flechon, C.; Danz, M.; Verma, A.; Navarro, J. M.; Zink, D. M.; Brase, S.; Baumann, T. From Iridium and Platinum to Copper and Carbon: New Avenues for More Sustainability in Organic Light-Emitting Diodes. *Green Chem.* **2015**, *17*, 1988.
(26) Dias, F. B.; Santos, J.; Graves, D. R.; Data, P.; Nobuyasu, R. S.; Fox, M. A.; Batsanov, A. S.; Palmeira, T.; Berberan-Santos, M. N.; Bryce, M. R.; Monkman, A. P. The Role of Local Triplet Excited States and D-A Relative Orientation in Thermally Activated Delayed Fluorescence: Photophysics and Devices. *Adv. Sci.* **2016**, 3, 1600080.
(27) Nobuyasu, R. S.; Ren, Z.; Griffiths, G. C.; Batsanov, A. S.; Data, P.; Yan, S.; Monkman, A. P.; Bryce, M. R.; Dias, F. B. Rational Design of TADF Polymers Using a Donor–Acceptor Monomer with Enhanced TADF Efficiency Induced by the Energy Alignment of Charge Transfer and Local Triplet Excited States. *Adv. Opt. Mater.* **2016**, *4*, 597.

TOC Graphic.

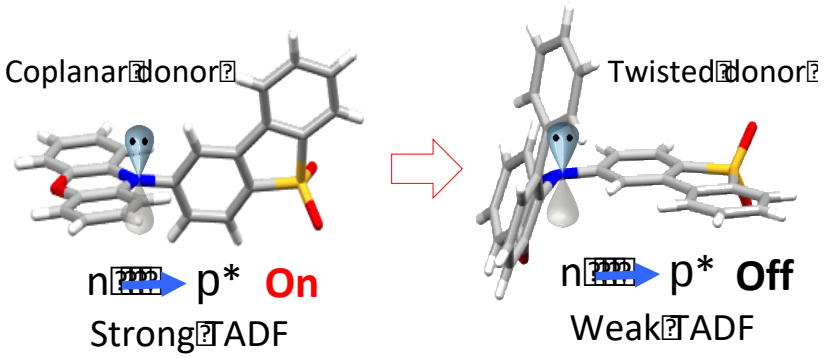
Coplanar donor
n p* On
Strong TADF
Twisted donor
n p* Off
Weak TADF